
Article:
Kuponu, O.S, Kadirkamanathan, V., Bhattacharya, B. et al. (1 more author) (2016) Using feedback control to actively regulate the healing rate of a self-healing process subjected to low cycle dynamic stress. Smart Materials and Structures, 25 (5). 55028. ISSN 0964-1726

https://doi.org/10.1088/0964-1726/25/5/055028

Using Feedback Control to Actively Regulate the Healing Rate of a Self-Healing Process Subjected to Low Cycle Dynamic Stress

O.S. Kuponu[1], V. Kadirkamanathan[1], B. Bhattacharya[2], S.A. Pope[1]

[1]Department of Automatic Control and Systems Engineering, University of Sheffield, Mappin Street, Sheffield, S1 3JD, UK

[2]Department of Mechanical Engineering, Indian Institute of Technology Kanpur, Kanpur, India

E-mail: oskuponu1@sheffield.ac.uk

Abstract. Intrinsic and extrinsic self-healing approaches through which materials can be healed generally suffer from several problems. One key problem is that to ensure effective healing and to minimise the propagation of a fault, the healing rate needs to be matched to the damage rate. This requirement is usually not met with passive approaches. An alternative to passive healing is active self-healing, whereby the healing mechanism and in particular the healing rate, is controlled in the face of uncertainty and varying conditions. Active self-healing takes advantage of sensing and added external energy to achieve a desired healing rate. To demonstrate active self-healing, an electrochemical material based on the principles of piezoelectricity and electrolysis is modelled and adaptive feedback control is implemented. The adaptive feedback control compensates for the insufficient piezo-induced voltage and guarantees a response that meets the desired healing rate. Importantly, fault propagation can be eliminated or minimised by attaining a match between the healing and damage rate quicker than can be achieved with the equivalent passive system. The desired healing rate is a function of the fault propagation and is assumed known in this paper, but can be estimated in practice through established prognostic techniques.

1. Introduction

Improvements in schedule and condition monitoring have gone a long way to keeping working environments safe and prolonging system usage. More so, profit returns on system utility has been maximised. However, these forms of monitoring and maintenance do not come without limitations in some applications. For example, the fragmentation of an in-flight passenger aircraft [1] and the loss of a wing panel of an in-flight passenger aircraft [2] resulted from negligence and the development of an incipient crack respectively. Wear and tear is also a factor that can lead to catastrophic events; this indicates the need for a more robust approach (temporary or permanent), particularly for systems that cannot be easily stopped or accessed during operation. A shift to a

self-healing approach that takes remedial action has the benefits of improved safety, longevity, profits, reliability and material lightness to industries such as aerospace, automotive, civil, etc. [3, 4]. Self-healing is the ability of a material to regain all or some level of its previous functionality or material properties after experiencing shock or damage. The approach to regaining functionality makes it different from fault tolerance, which isolates the anomaly while devising suboptimal approaches (such as redundancy and reconfiguration) to regain some performance. Self-healing eliminates the anomaly through repair and recovers functionality.

One may argue that the technology readiness level (TRL) of self-healing materials is between TRL-1 (basic concept) to TRL-3 (laboratory) [5]. Still, research on self-healing materials is ongoing and a lot of interest has been shown from companies and the research community [3, 4, 6–9]. Lightness, durability, affordability and the ability to combine with other materials, make composite materials particularly suitable for self-healing. Composite materials with self-healing capabilities restore mechanical properties like Young's modulus, tensile strength etc. in the event of anomalies such as fibre cracks, delamination, matrix crack and fibre-matrix debonding [6, 7]. This is achieved by storing healing agents in the materials without altering the mechanical properties of the material. In the event of damage, the healing agent is triggered and released into the damage zone to recover functionality [10]. Typically, self-healing comes in extrinsic or intrinsic form. The latter is a chemical based approach where healing of the intrinsic material is achieved through thermally reversible reactions, use of thermoplastic, hydrogen bonding, ionomeric coupling, molecular diffusion and chain interlocking [5, 10]. Common reversible reactions include Deils-Ader(DA) and retro-Deils-Alder(rDA) initiated by some form of energy e.g. heat to polymerise damaged areas. Experiments have been performed within a temperature range of 100°C to 150°C to initiate self-healing using DA or rDA reactions of multi-furan and multi-meleimide after damage has occurred [5, 8, 11, 12].This has also found application in ballistics where the heat generated from a fired bullet passing through an elastomer is used to intrinsically mend the depleted region [3]. The self-healed polymer showed improved tensile and compressive strength when compared with damaged polymer. In an attempt to reduce the high energy limitation of a thermally reversible reaction, a moderately driven thermal approach using disulphide chemistry during covalent bonding to mend the damaged area was presented [13]. Another method of intrinsic self-healing is to use thermoplastic as the healing agent, which is initiated in a polymeric composite material by heat. The melting thermoplastic flows to the damaged area to mix with the matrix material. Several studies of this method have shown high percentage of mechanical recovery [14–16]. A possible setback to this thermoplastic approach is the high viscosity of the selected thermoplastic resin. The healing agent must flow as fast as possible to improve the healing rate and subsequently negate the effect of the damage rate [10]. One way to overcome high viscosity is to increase the temperature and choose healing agents with low viscosity. Overall, intrinsic self-healing is generally restricted to a small damage zone [13] and as such has limited applications. Also, a trigger which most of

the time is externally supplied, is required to initiate healing and does not necessarily make this approach autonomous.

On the other hand, extrinsic self-healing is architecturally designed to store separate healing agents in vascular networks or capsules in the material. The capsule based method is such that enclosed capsules housing the healing agents are placed in the composite material. Damage to the material leads to rupture of the capsules and bleeding of the healing agent to the damage area. Different studies [17–21] have applied this approach and sometimes a catalyst is required to speed up healing. In one study, microcapsules of calcium lactate and bacteria(catalyst) were placed in a cementitious composite [9]. The process of self-healing begins when a crack occurs in the concrete, and with the aid of water, the calcium lactate bleeds through and reacts with the bacteria to form limestone in the cracked region. Further investigation has also shown how different pH level affects the triggering and release of healing capsule placed in a concrete [22]. Other examples of healing agents enclosed in microcapsules are dicyclopentadiene [23], rapeseed oil [24] and fluorescent fluid [25]. Also, microcapsules containing a mixture of strontium fluoroaluminosilicate and polyacrylic acids [26] and another containing Triethylene glycol dimethacrylate-N and N-dihydroxyethyl-p-toluidine [27] were recorded in dental application. While toxic concerns have been raised with some microcapsule contents [28, 29], the later is deemed safe for dental application [27]. It is expected that more functional applications will emerge particularly with the success in embedding microcapsules in a polyelectrolyte multilayer [30]. The number of times healing can be initiated in capsule based self-healing is dependent on the number of capsules placed in the material. This places a limitation on applicability, particularly for materials subjected to continuously harsh conditions. Vascular based approaches use capillaries or hollow tubes constructed in one, two or three dimensions to house the healing agents. Increased dimensionality adds a higher degree of reliability, flexibility and increases the number of times healing is initiated, since the damaged area has multiple connectivity to the healing agent. A capillary tube containing thiol-alkyne click chemistry was placed in a rubber matrix to form a composite [10]. During fracture, the reactant bleeds into the damaged area where a reaction stimulated by UV light quickens the healing rate. After 5 minutes of exposure, an increase of up to 30% was recorded for the Young's modulus and 100% in 10 minutes when compared to the damaged composite.

The majority of progress in self-healing remains passive and reactive to damage. This means that there is no measure of capturing the incipient cause of damage, no guarantee of matching the healing rate to the damage rate and healing is passively initiated only after damage occurs. Nonetheless, a few works have reported integration of sensing into self-healing processes with the aim of improving the reliability of local detection, diagnosis and efficiency of healing (see table 1 for a summary) [7, 31–36]. A damage detection system consisting of a pressure sensor located in a pressurised vascular network and whose output was monitored through a microprocessor was used to trigger the delivery of healing resin from an external reservoir when a crack occurs [7].

Table 1. Some self-healing approaches with integrated sensing capabilities

Sensing Type	Damage Detected	Self-healing System	Material Healed
Pressure	Delamination, microcracks	Vascular	FRP [7]
Fibre Optics	Delamintion	Vascular	CFRP [31]
Pressure sensor	Cracks, delamination, debonding	Vascular	CFRP [33]
Photo-resistor	Cracks	Intrinsic	TP [32]
Acoustic emission	Cracks	Vascular	Epoxy [34, 35]
Acoustic emission	Cracks	Intrinsic	TP [36]

FRP - Fibre reinforced plastic
CFRP Carbon fibre reinforced plastic
TP-Thermoplastic polymer

Distributed fibre sensors mounted on a composite plate to detect the pressure drop and initiate the supply of healing agent from an external source has also been reported [31]. In addition to the integrated sensing, an intrinsically driven self-healing material was developed with controlled triggering and healing mechanisms [32]. This consists of a high resistive alloy wire placed in an ethylene vinyl acetate (EVA) thermoplastic material to act as the healing agent. Unlike the other intrinsic approaches, a photo-resistive sensor gathers information on the light level. A voltage drop indicates an increased intensity of light and crack size. With a given voltage threshold four standard deviations less than the mean value of a damage free training set, detection analysis is carried out. Based on the analysis, current is passed through the wire to melt the EVA in the damaged region to seal the crack. Once the photo-resistive sensor records a voltage at the same level as the set voltage threshold, the current stops flowing and the healing process stops. This closed loop approach introduces some form of controlled on/off regulation of the self-healing mechanism.

An interesting approach is the potential of using electromechanical materials in self-healing systems. These are materials that can convert mechanical energy into electrical energy and vice-versa, such as piezoelectric materials. The potential of such materials is that they can be used as actuators and sensors. Polymers currently used that exhibit such characteristics are Lead Zirconate Titanate (PZT), poly vinylidene fluoride (PVDF) and dielectric elastomers [13, 37]. Two studies prepared poly vinylidene fluoride-co-hexafluropropylene (PVDF-HFP) solid electrolyte by mixing PVDF-HFP, zinc oxide and copper nanoparticles together [6,38]. This was combined with carbon fibre reinforcement to form a composite laminate. Both experiments showed how a healing agent (i.e. copper nanoparticles) can be deposited within a crack zone by combining the principle of the piezoelectric direct effect and solid state electrolysis. The piezoelectric effect generates a voltage when the material is subjected to concentrated stress. The voltage generated triggers the electrolysis process, leading to deposition of the healing agent. Like other self-healing approaches, this material faces the challenge of balancing the healing and damage rate. In this arrangement, self-healing is only possible when the piezo-induced potential energy is greater than the inherent over-potentials of electrolysis. Only then is the charge sufficient to drive the electrochemical mass at a high rate. In practice, materials are subject to varying stress level over time and the stress may not generate enough potential energy to drive the healing process. Also, another inherent problem is

the duration of deposition of the healing agent. The piezo-induced energy must be able to sustain the required duration of deposition of the healing agent to ensure adequate healing. All of these problems affect the rate of deposition of the healing agent.

With the current self-healing approaches, the generally poor match between the healing and damage rate undermines the performance and effectiveness of self-healing. By using an active self-healing system, healing can be controlled and regulated effectively. This ensures reliability and improved recovery from the effect of damage. To demonstrate the effectiveness of the proposed approach to constant and varying perturbation, an electromechanical material that has previously been experimentally demonstated [6, 38] has been modelled and simulated. This paper then shows how adaptive feedback control can compensate for the insufficient potential energy driving the self-healing and can guarantee a response that will match the effect of fault propagation in the simulated system. A match between the damage and healing rate is achieved, which improves the performance of self-healing in minimising or eliminating fault propagation.

2. The Concept of Active Self-healing

Figure 1 describes a typical self-healing process of a composite material. These designs can suffer from several inherent limitations such as:

1. Generally, healing is initiated passively and does not take into account the propagation of a fault to detect the damage at an early stage and initiate healing. In addition, taking into account the propagation of a fault allows one to introduce a tolerant system and limit the number of times healing takes place, thus maintaining the availability of healing agents.
2. Self-healing is typically an open loop process with no regulation of the healing process to counteract the onset of damage. As a result, the process might be unable to achieve the desired healing response and handling of uncertainty/disturbance is also likely to be poor.
3. There is usually no controllable mechanism to terminate the process. For example, healing agent stops bleeding into the damaged zone when flow is restricted.

To tackle these limitations, self-healing should be addressed from a multidisciplinary perspective to enhance performance and improve the technology readiness of self-healing systems [39]. One of such example is to introduce active control and prognosis into a self-healing material. This concept is shown in figure 2 and is referred to as active self-healing. Active control is a process through which external energy is applied to a process to achieve a desired response. Prognostic techniques help to locate the damage and to define a desired response by taking advantage of sensor measurements to estimate a measure of the damage rate. Regulating the healing rate involves controlling factors that can affect the reaction kinetics of a healing process. Factors such as the speed of delivery/mass flow rate [40], release mechanism, temperature, catalyst, pressure,

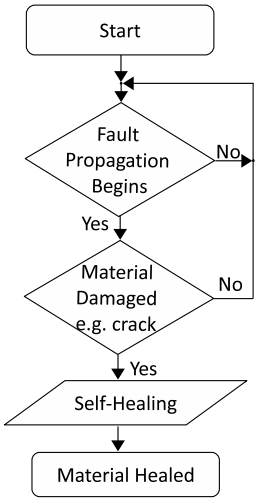

Figure 1. Typical self-healing process of a composite material.

concentration and pH level vary from system to system. For example, feedback control can be applied to a vascular network to control the pressure release and flow rate of healing agent from an external reservoir. Integrated sensing within the network gathers information that is sent to the prognostics unit for analysis. Based on the location and quantification of damage, the feedback control works to deliver the desired release and flow rate that will negate the effect of damage. The behaviour of the release and flow of healing agent in such a system has previously been modelled [41]. In self-healing of a cementitious composite, the pH level has been determined to affect the release rate of healing agents enclosed in microcapasules [22] and can be controlled to give a desired response with respect to the effect of damage. In the intrinsic self-healing simulated in this paper, the piezo-induced energy has been identified as a limit to the chemical kinetics of an electrolytic process. The aim is to maintain a sufficient chemical kinetic by controlling the piezo-induced energy based on the analysis of the prognostics unit. The advantages of this complete closed loop system are that it allows for pre-emptive healing, regulation of the healing process and a proper match between the healing and damage rate. This means that a desired response can then be achieved regardless of any disturbance or uncertainty that may affect the performance of the healing process. Active self-healing addresses some of the shortfalls of a typical self-healing process, can guarantee a high degree of reliability and has the potential to improve the level of confidence in accepting a self-healing material for everyday use.

3. Introduction and Modelling of a Self-healing Electromechanical Composite Material

Experiments have previously been carried out to show the potential of using an electromechanical material for self-healing [6, 38]. Poly vinylidene fluoride-co-hexafluropropylene (PVDF-HFP), zinc oxide and copper nanoparticles were mixed

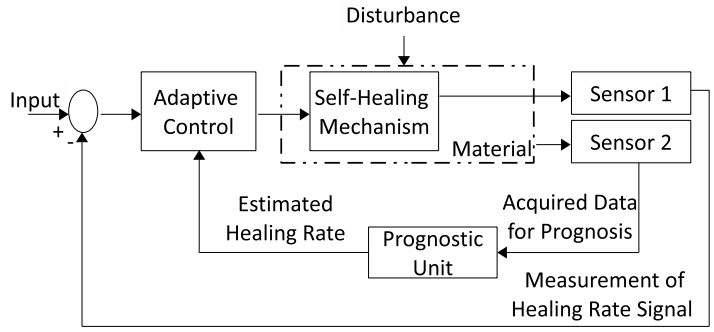

Figure 2. Introducing a generic concept of active self-healing of a composite material. The input is defined as what drives the healing system e.g. force, pressure, power, heat etc.

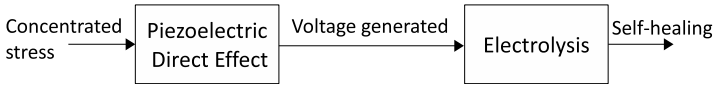

Figure 3. Open-loop representation of self-healing process of the material showing the principle of operation.

together to form a PVDF-HFP solid electrolyte. Carbon fibre reinforcement and the PVDF-HFP solid electrolyte were combined in alternating layers to form composite laminates and held together by bolts which also act as electrodes. This newly formed composite material exhibits self-healing properties. Figure 3 depicts the principle behind the self-healing process. Sustained stress applied in the vicinity of the electrode generates a voltage due to the piezoelectric direct effect phenomenon. The applied stress can cause a crack in the material. However, the generated voltage is used to actuate the electrolysis process which deposits copper nanoparticles in the crack region. To validate the self-healing at the cracked area, a mechanical test measuring the hardness of the material was carried out. The result showed increased material strength with the deposition of copper in the cracked area when compared to no deposition.

As this open loop self-healing process is driven by a voltage, it is particularly suitable to be developed into an active self-healing process that is regulated by some form of digital feedback control. To begin, the principle of operation behind the self-healing process is modelled by two subsystems. The piezoelectric subsystem models the electromechanical property of the material in section 3.1, and the deposition of healing agent is modelled through the electrolysis subsystem in section 3.2.

3.1. Electromechanical Model of the Piezoelectric Subsystem

Piezoelectric materials can be used in two ways. The piezoelectric direct effect converts mechanical energy into electrical energy while the converse effect is the reverse of this. Figure 4 shows a piezoelectric stack consisting of n layers of piezoelectric patch material connected in parallel. The stack is used to enhance charge generation when compared

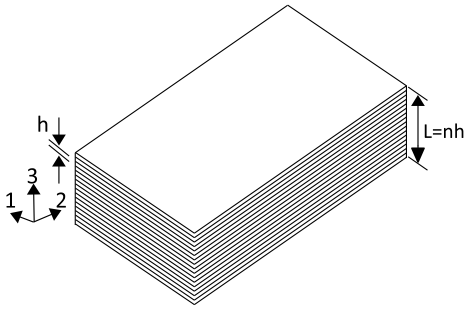

Figure 4. Stacked piezoelectric material consisting of n layers of piezoelectric patch.

to a bulk piezoelectric. The constitutive relations in the transverse direction of a piezoelectric stack are shown in (1) - (2). These couple the mechanical and electrical response of a stacked piezoelectric material [42–47].

$$S_3(t) = s_{33}^E T_3(t) + d_{33} E_3(t) \tag{1}$$

$$D_3(t) = d_{33} T_3(t) + \epsilon_{33}^T E_3(t) \tag{2}$$

Mechanical energy applied to a piezoelectric material induces an electric field E_3 in the material. The piezoelectric direct effect defined in (2) describes the resulting electrical characteristics and their relation to an applied mechanical stress. Similarly, (1) is the piezoelectric converse effect which defines the mechanical characteristics and their relation to an applied electric field. S_3 and D_3 are the strain and electric displacement respectively, s_{33}^E and ϵ_{33}^T are the compliance constant and dielectric permittivity respectively, d_{33} represents the piezoelectric coupling coefficient, T_3 is the stress and E_3 is the electric field. The relationships between the voltage V across each piezoelectric layer, the total charge Q generated from electric displacement and other parameters are given in (3).

$$V = hE_3; \quad Q = nD_3A; \quad S_3(t) = \frac{x(t)}{L}; \quad s_{33}^E = \frac{1}{E}; \quad T_3(t) = \frac{f}{A} \tag{3}$$

Where f is the stack actuator force, E defines the Young's modulus, A is the cross-sectional area of the piezoelectric material, $x(t)$ represents the relative stack displacement, n is the number of piezoelectric layers, h is the thickness of a piezoelectric patch and L is the total height of the stack given as $L = nh$. Substituting (3) into (1) - (2) results in (4) - (5).

$$x(t) = \frac{L}{EA} f(t) + d_{33} n V(t) \tag{4}$$

$$Q(t) = d_{33} n f_s(t) + \frac{n\epsilon_{33}^T A}{h} V(t) \tag{5}$$

The total capacitance, stiffness and applied force of the piezoelectric stack are given as $C = \frac{n\epsilon_{33}^T A}{h}$, $k = \frac{EA}{L}$ and $f(t)$ respectively. Equation (4) - (5) is rewritten to emphasize

the direct relationship between the applied force and charge by reversing their polarities in (6) - (7).

$$x(t) = -\frac{1}{k}f(t) + d_{33}nV(t) \tag{6}$$

$$-Q(t) = d_{33}nkx(t) + CV(t) \tag{7}$$

On differentiation and substitution for $\dot{Q}(t) = \frac{V}{R}$ (where R is the total resistance of the stack), (7) becomes (8).

$$\dot{V}(t) = -\frac{1}{RC}V(t) - \frac{d_{33}nk}{C}\dot{x}(t) \tag{8}$$

Equation (6) represents the mechanical model coupled with electrical signal for a massless system. Taking into account the mass of the piezoelectric stack which is not negligible, the sum of the forces acting on the piezoelectric stack is equal to the inertial force due to the mass. This assumes a simple lumped mass single degree of freedom (SDOF) model and (6) becomes (9).

$$M\ddot{x}(t) = -kx(t) + d_{33}nkV(t) - f(t) \tag{9}$$

$$\ddot{x}(t) = -\frac{1}{M}\Big(kx(t) - d_{33}nkV(t) + f(t)\Big) \tag{10}$$

Equation (11) - (12) give the state-space representation of (8) and (10).

$$\begin{pmatrix} \ddot{x} \\ \dot{x} \\ \dot{V} \end{pmatrix} = \begin{pmatrix} 0 & -\frac{k}{M} & \frac{d_{33}nk}{M} \\ 1 & 0 & 0 \\ -\frac{d_{33}nk}{C} & 0 & -\frac{1}{RC} \end{pmatrix} \begin{pmatrix} \dot{x} \\ x \\ V \end{pmatrix} + \begin{pmatrix} -\frac{1}{M} \\ 0 \\ 0 \end{pmatrix} f(t) \tag{11}$$

$$y = \begin{pmatrix} 0 & 0 & 1 \end{pmatrix} \begin{pmatrix} \dot{x} \\ x \\ V \end{pmatrix} \tag{12}$$

3.2. Model of Electrolysis Subsystem

For simplicity and understanding of the principle of electrolysis, a simple model of the relationship between the applied voltage and current flowing during electrolysis is adopted [48]. A setup for electrolysis requires electricity, electrodes and electrolyte. These requirements are met by the voltage generated through the piezoelectric direct effect, the bolt joining the composite laminates and the PVDF-HFP solid electrolyte respectively. The voltage generated causes ionic transportation of copper to the crack area. More so, ionic transportation only occurs when the generated voltage is sufficient to overcome inherent barriers in electrolysis. These barriers include the reversible potential of the electrolyte, over-potential of the electrodes and the ohmic and membrane resistance. In this model, emphasis is on current flowing through an electrolytic process. This current is proportional to the deposition rate and can easily be measured during

experiment. The minimum voltage that is required from the electromechanical material to actuate the electrolysis process is expressed in (13).

$$V_{min} = E_{rev} + IR \tag{13}$$

Where E_{rev} is the reversible potential and the other barriers are coupled into the resistance R. Equation (14) - (15) represents the power used during electrolysis.

$$P \propto (V - E_{rev} - IR)^2 \tag{14}$$

$$P = K(V - E_{rev} - IR)^2 \tag{15}$$

Considering the power loss I^2R due to the internal resistance of the material, (15) becomes (16).

$$IV - I^2R = K(V - E_{rev} - IR)^2 \tag{16}$$

$$I = \frac{V + 2KR(V - E_{rev}) - \sqrt{V^2 + 4KRE_{rev}(V - E_{rev})}}{2R(1 + KR)} \tag{17}$$

Equation (17) is a mathematical representation of the relationship between the voltage applied and the actual current flowing during electrolysis and is derived from (16). The piezo-induced voltage must be sufficient to generate enough current flow to initiate ionic transportation. This implies that there is either a current flow or not. Defining these two possibilities as regions, (17) is simplified further for modelling purposes. The current flowing during electrolysis is represented in (18) using the first order linear approximation of (17).

$$I(t) = \begin{cases} m(V(t) - E_{rev}) & \text{for } V(t) > E_{rev} \\ 0 & \text{for } V(t) \leq E_{rev} \end{cases} \tag{18}$$

Equation (18) can be expressed in the manner of (19).

$$I(t) = mV(t) + \Delta I(t) \tag{19}$$

$$\Delta I(t) = \begin{cases} -mE_{rev} & \text{for } V(t) > E_{rev} \\ -mV(t) & \text{for } V(t) \leq E_{rev} \end{cases} \tag{20}$$

m is a positive slope within the bounds $[m_{min}\ m_{max}]$. E_{rev} is assumed to be unknown, but $E_{rev} > 0$ and $E_{rev} \in [E_{revmin}\ E_{revmax}]$.
Since $\dot{Q}(t) = I$, the system is formulated in terms of $\dot{Q}(t)$ for the purpose of designing the controller in the next section. Hence, (19) is rewritten as (21).

$$\dot{Q}(t) = mV(t) + \Delta I(t) \tag{21}$$

The relationship between the voltage input and the current flow represents a deadzone and is shown in figure 5. While the system is operating in the deadzone region($V(t) \leq E_{rev}$), the self-healing process experiences a definite mismatch between the healing and damage rate. In practice, composite materials are subjected to varying stress levels and are often harmonic signals. Therefore, they may not generate sufficient voltage to consistently initiate the self-healing process. Insufficient piezo-induced voltage implies that the process becomes insensitive to the input and generates no current.This inevitably affects the self-healing performance.

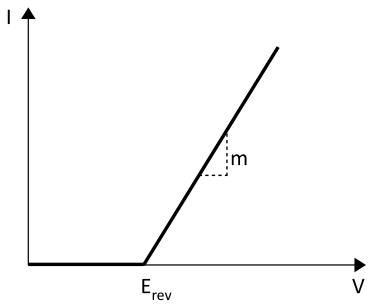

Figure 5. Current flowing during self-healing can be represented as a deadzone model. Piezo-induced voltage below E_{rev} generates no current flow.

4. Control Design

The non-linear deadzone is an inherent problem identified in section 3.2 that undermines the performance of this self-healing mechanism. For these kinds of non-linear systems, conventional feedback control will have varying performance. As the controller will be designed with fixed gains, it is unlikely to achieve the desired performance when faced with the change in dynamics resulting from the deadzone, thus making it unsuitable for this application. A robust control design can be implemented but outside the designed bounds, unaccounted variation can affect the performance of the system. However, adaptive control has been implemented for these class of system and results have shown that a desired response can be achieved [49–51]. An adaptive controller evolves by generating new control gains over time so as to drive the mismatch between a desired response and the actual system response to zero.

In this section, an adaptive controller is implemented to compensate for the variation and insufficient magnitude of the piezo-induced driving voltage, while guaranteeing a suitable self-healing performance. The control objective is for the actual current ($\dot{Q}_a$) during electrolysis to track a desired current ($\dot{Q}_d$) for the self-healing process. The desired current ($\dot{Q}_d$) is in effect a function of the desired healing rate for the process. While the controller gains are revaluated, it is essential that the system is not driven to a state of instability. As such, an adaptive sliding mode controller(SMC) is designed to ensure stability, fast response and robustness. The control design involves choosing a surface ($s = 0$) and designing a control law $U(t)$ such that the system trajectory slides to the surface. This procedure ensures that the tracking error between the actual and desired current is zero. Two cases are considered in the control design based on the previous mathematical formulation [52–55]:

- Case I: An isolated electrolytic process regulated by a feedback control law.
- Case II: A piezo-electrolytic process regulated by a feedback control law.

The significance of cases I in figure 6(a) is to show how a feedback control law can be used to regulate the non-linear self-healing process. Then more importantly from

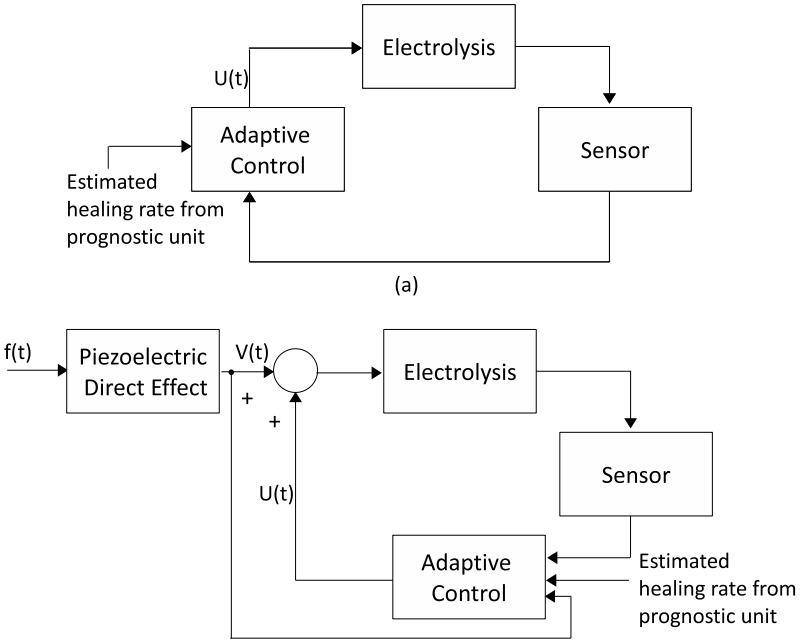

Figure 6. Two instances of adaptive feedback control implementation: (a) Case I - An isolated electrolytic process to demonstrate how a non-linear self-healing process can be regulated by adaptive feedback control. (b) Case II - A piezo-electrolytic process to show how adaptive feedback control can regulate an integrated sensing and non-linear self-healing process that is subject to constant and varying stress input.

an application perspective, case II in figure 6(b) demonstrates how feedback control can regulate an integrated sensing and non-linear self-healing process that is subject to varying stress input over time.

4.1. Case I: Isolated Electrolytic Process Regulated by a Feedback Control Law

Regardless of the initial conditions of the system trajectory, (22) represents a surface ($s = 0$) on which the system trajectory slides to at a finite time and the tracking error exponentially decays to zero.

$$s(t) = \lambda \tilde{Q}(t) \tag{22}$$

The term λ is a strictly positive constant, $\tilde{Q} = Q_a(t) - Q_d(t)$ and the derivative of $\tilde{Q}$ is the tracking error. This suggests that the surface ($s = 0$) has a unique solution $\tilde{Q}(t) = 0$. To design a control law $U(t)$, (22) is differentiated and $U(t)$ is introduced.

$$\dot{s}(t) = \lambda \dot{\tilde{Q}}(t) = \lambda(\dot{Q}_a(t) - \dot{Q}_d(t)) \tag{23}$$

Substituting (21) into (23) gives (24). Also, for this case the control input $U(t) = V(t)$, i.e. the voltage.

$$\dot{s}(t) = \lambda(mU(t) + \Delta I(t) - \dot{Q}_d(t)) \tag{24}$$

By designing a control law $U(t)$ that satisfies the condition $\frac{1}{2}\frac{d}{dt}s^2 \leq -\eta|s|$, the surface $s(t)$ is kept at zero. This condition means that for all system trajectories, the squared

distance to the surface is non-increasing. The control law $U(t)$ is expressed in (25).

$$U(t) = -K_d s(t) - \frac{\Delta I(t)}{m} + \frac{1}{m}\dot{Q}_d(t) - \eta sgn(s(t)) \tag{25}$$

Where η and K_d are positive constants. To eliminate the chattering phenomenon introduced by the sign function, the tuning error s_ϵ in (26) replaces the surface $s(t)$.

$$s_\epsilon = s - \epsilon sat\Big(\frac{s}{\epsilon}\Big) \tag{26}$$

where $sat(z) = \begin{cases} 1 & \text{for } z \leq 1 \\ z & \text{for } -1 < z < 1 \\ -1 & \text{for } z \leq -1 \end{cases}$

The control law $U(t)$ becomes (27).

$$U(t) = -K_d s(t) + \hat{\phi}\dot{Q}_d(t) - k^* sat\Big(\frac{s}{\epsilon}\Big) \tag{27}$$

The control law (27) assumes that $1/m$ is unavailable but $\hat{\phi}$ is the estimate of $\phi \triangleq [1/m]$ and $\tilde{\phi} = \hat{\phi} - \phi$. Also, $\Delta I(t)$ is bounded by $\Delta I(t) \leq \rho$ and $k^* \geq \rho/m_{min}$. ρ is defined as $m_{max}E_{revmax}$ and $k^* sat(s/\epsilon)$ introduces robustness that compensates for $\Delta I(t)$. A stable adaptive law can be evaluated using Lyapunov stability theory to ensure that the system is not driven to instability [52]. Equation (28) is the Lyapunov candidate W that has been selected and the derivative of W along the system trajectory is expressed in (29).

$$W(t) = \frac{1}{2}\Big(\frac{1}{m}s_\epsilon^2 + \frac{1}{\gamma}\tilde{\phi}^2\Big) \tag{28}$$

$$\dot{W}(t) = \frac{1}{m}s_\epsilon \dot{s} + \frac{1}{\gamma}\tilde{\phi}\dot{\hat{\phi}} \tag{29}$$

Equation (24) and (27) are substituted into (29) to give (30).

$$\dot{W}(t) = -\lambda K_d s_\epsilon s + \lambda s_\epsilon\Big(\hat{\phi}\dot{Q}_d(t) - k^* sat\Big(\frac{s}{\epsilon}\Big)\Big) + \lambda s_\epsilon\Big(\frac{\Delta I(t)}{m} - \phi\dot{Q}_d(t)\Big) + \frac{1}{\gamma}\tilde{\phi}\dot{\hat{\phi}} \tag{30}$$

Substituting the adaptive law (31) into (30) gives the expression in (32).

$$\dot{\hat{\phi}} = -\gamma\lambda\dot{Q}_d(t)s_\epsilon \tag{31}$$

$$\dot{W}(t) = -\lambda K_d s_\epsilon s - \lambda k^* s_\epsilon sat\Big(\frac{s}{\epsilon}\Big) + \frac{\Delta I(t)}{m}\lambda s_\epsilon \tag{32}$$

$$\dot{W}(t) = -\lambda K_d s_\epsilon\Big(s_\epsilon + \epsilon sat\Big(\frac{s}{\epsilon}\Big)\Big) - \lambda k^* s_\epsilon sat\Big(\frac{s}{\epsilon}\Big) + \frac{\Delta I(t)}{m}\lambda s_\epsilon \tag{33}$$

When $|s| \leq \epsilon$, $|s_\epsilon| = 0$ and (33) is zero (34).

$$\dot{W}(t) = 0 \qquad\qquad \forall |s| \leq \epsilon \tag{34}$$

When $|s| > \epsilon$, $|s_\epsilon| = s_\epsilon sat(s/\epsilon)$. By also taking into account $k^* \geq \rho/m_{min}$, (33) is expressed to give (37).

$$\dot{W}(t) = -\lambda K_d s_\epsilon^2 - (K_d\epsilon + k^*)\lambda|s_\epsilon| + \frac{\Delta I(t)}{m}\lambda s_\epsilon \tag{35}$$

$$\dot{W}(t) \leq -\lambda K_d s_\epsilon^2 - K_d \epsilon \lambda |s_\epsilon| - \Big(k^* - \frac{\Delta I(t)}{m}\Big)\lambda |s_\epsilon| \tag{36}$$

$$\dot{W}(t) \leq -\lambda K_d s_\epsilon^2 \qquad \forall |s| > \epsilon \tag{37}$$

The above formulations in (34) and (37) indicate that s_ϵ and $\tilde{\phi}$ are globally bounded. This also means that $s(t)$ is bounded and the control design guarantees that the system trajectory will converge to the sliding mode.

4.2. Case II: Piezo-Electrolytic Process Regulated by a Feedback Control Law

Consider a composite material system whose self-healing is driven by a piezo-electrolytic process. The performance of self-healing is limited by the inherent deadzone nonlinearity of the system and the insufficient piezo-induced voltage $V(t)$ that drives the healing agents. An adaptive feedback controller in figure 6(b) is designed to regulate the self-healing process by overcoming the inherent deadzone and ensuring a proper match between healing and damage rate.

The system model (21) is modified by adding a feedback control law $U(t)$ to give Equation (38).

$$\dot{Q}_a(t) = m(V(t) + U(t)) + \Delta I(t) \tag{38}$$

Following the design from section 4.1, the derivative of the surface $\dot{s}(t)$ and the control law $U(t)$ are expressed as (39) and (40) respectively.

$$\dot{s}(t) = \lambda m(V(t) + U(t)) + \lambda \Delta I(t) - \lambda \dot{Q}_d(t) \tag{39}$$

$$U(t) = -K_d s(t) - \hat{V} + \hat{\phi}\dot{Q}_d(t) - k^* sat\Big(\frac{s}{\epsilon}\Big) \tag{40}$$

$V(t)$ and ϕ are unknown during the control design but are estimated as $\hat{V}$ and $\hat{\phi}$ respectively. Hence, $\tilde{V} = \hat{V} - V$ and $\tilde{\phi} = \hat{\phi} - \phi$. Based on a similar formulation to section 4.1, the Lyapunov candidate and the adaptive laws are given in (41) - (43). Details of the formulation can be found in the supplementary material.

$$W(t) = \frac{1}{2}\Big(\frac{1}{m}s_\epsilon^2 + \frac{1}{\gamma}\tilde{\phi}^2 + \frac{1}{\Gamma}\tilde{V}^2\Big) \tag{41}$$

$$\dot{\hat{\phi}} = -\gamma \lambda \dot{Q}_d(t) s_\epsilon \tag{42}$$

$$\dot{\hat{V}} = \lambda \Gamma s_\epsilon \tag{43}$$

Again, this formulation indicates a global boundedness and the control design guarantees that the system trajectory will converge to the sliding mode.

Table 2. Properties of a typical electromechanical material

Parameter	Value	
Modulus E	$44GPa$	[43]
Piezoelectric coupling d_{33}	-24pC/N	[56]
Resistance R	19.2kΩ	[43]
Capacitance C	1.59μF	[43]
Cross-sectional area$A$	25mm^2	[43]
Stack Length L	16mm	[43]
Mass M	2.3g	[43]
Number of layers n	130	[43]
E_{rev}	680mV	[38]
Slope m	0.03	
m_{min}	0.01	
k^*	10	[Tuned]
K_d	50	[Tuned]
γ	0.5	[54]
ϵ	2.5	[Tuned]
λ	15	[Tuned]
Sample rate	0.005	

5. Simulation Results

In this section, the effectiveness of active self-healing is illustrated by simulating the two cases I & II. Some of the model parameters are chosen from literature, but the control and model parameters of the electrolytic process are primarily chosen with the aim of verifying the concept of active self-healing. These might not represent an actual system but they are indicative of typical material parameters. For any real system, their actual values (and those of some of the other parameters) would be identified from experimental data prior to the design of the controller. The parameters used are listed in table 2.

Case I:

To capture the changes in damage rate over time, a varying reference model is assumed. The varying reference is assumed to have direct proportionality to the damage rate. For an actual system, it can be obtained through appropriate prognosis and system identification techniques. Given that the damage rate of a material changes over time due to external conditions, a steady input will find it difficult to achieve a desired response. This is shown by applying voltages of $710mV$ and $510mV$ to the open-loop response of an isolated electrolytic process at different time instant. The result in figure 7(a) shows a poor mismatch between the actual current flow and the desired response due to the inherent deadzone non-linearity and the insufficient input. The performance of the adaptive SMC to the changing reference is shown in figures 7(a) and (b). The adaptive control law ensures that the actual current flow tracks the reference model. As the reference changes, the adaptive control law adjusts in order to achieve the primary tracking objective. Figure 7(b) shows a good tracking margin when the reference changes, but desirable performance is purely based on application. However, it is clear that the adaptive SMC in figure 7(c) is able to adapt to changes and ensure that tracking is regained. In terms of the self-healing process, the current flow is proportional to the rate of deposition, and achieving a desired current flow means that sufficient mass deposition of the healing agent is guaranteed. This inevitably negates the effect of damage. Tracking performance can be improved by carefully selecting the values of ϵ and

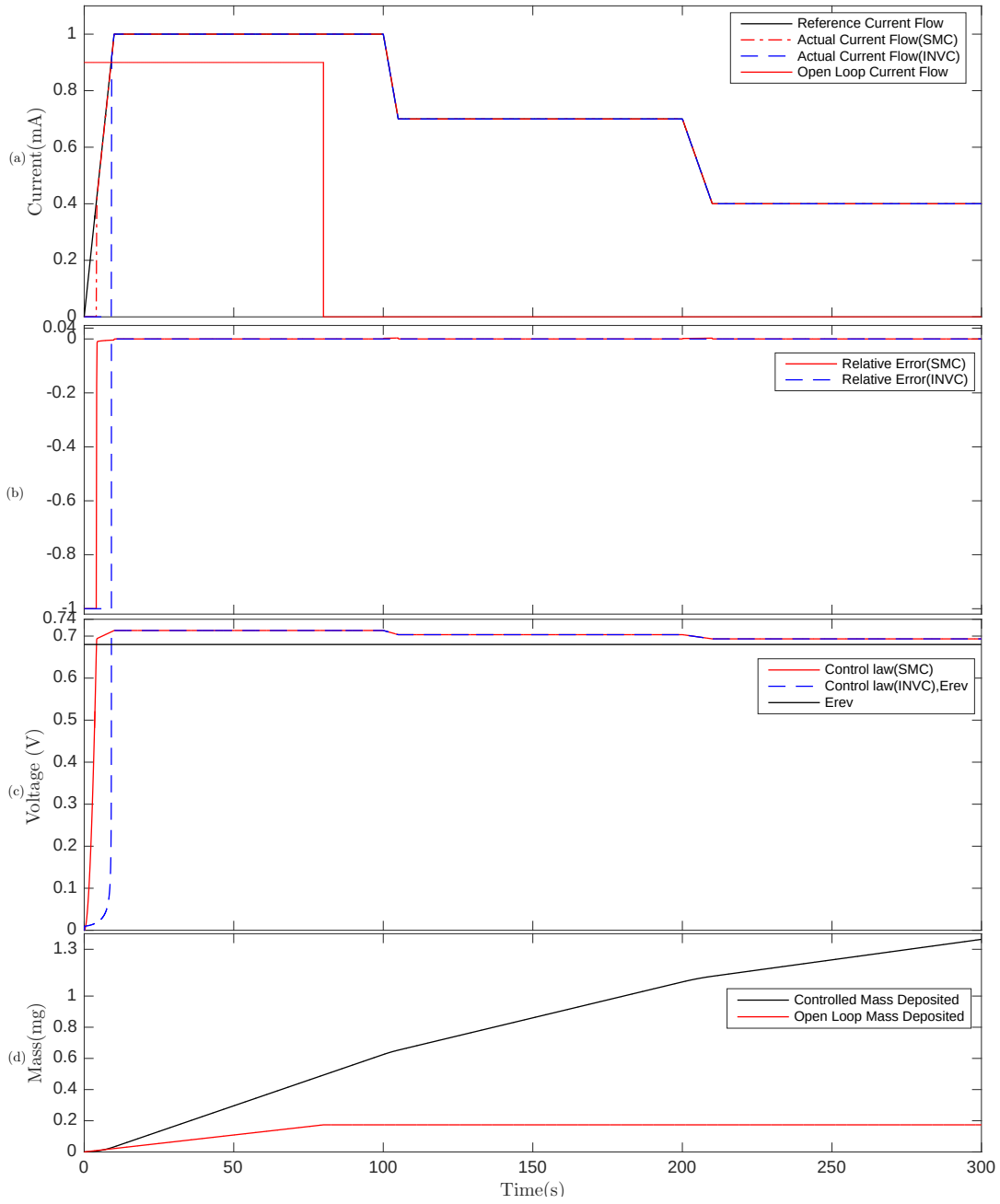

Figure 7. Case I - An isolated electrolytic process regulated by an adaptive feedback controller: (a) An adaptive SMC and INVC applied to an isolated electrolytic process to generate a desired current flow during electrolysis and a current flow from the open loop electrolytic process (b) Relative error of the adaptive SMC and INVC given as the difference between the actual and desired current divided by the desired current. (c) Adaptive SMC and INVC inputs applied to ensure tracking of the reference current flow. (d) The mass deposited over time.

λ, while ensuring that $\epsilon > 0$ to avoid chattering. The performance can be compared with an adaptive inverse controller (INVC) in figure 7(c) that ensures tracking of a reference signal by constructing an inverse deadzone to cancel the inherent deadzone [57]. Figure 7 suggests that the adaptive SMC has a better tracking of the reference model in the transient phase but both methods gave a good steady state performance. In addition, the mass deposited for the controlled and open loop system can be compared in figure 7(d), with about 685% increase in mass deposition recorded in 5 minutes for the controlled system. This generally suggests a better healing performance, but it is noted that the required amount of mass deposition is a function of the type and extent of fault. For example a larger crack would likely require greater mass deposition for effective healing.

Case II:

Case II relates to the composite material system, whose self-healing mechanism is based on piezo-electrolytic drive. These materials are subjected to constant and varying conditions. The conditions are simulated as sinusoidal input forces with constant and changing amplitudes respectively. A stress level of $12MPa$ is produced when a sinusoidal input force of amplitude $300N$ is applied at a frequency of $100rad/sec$ to the piezoelectric stack. The generated piezo-induced voltage is $559mV$ (see supplementary material for details). This demonstrates a situation where the material is subjected to constant condition. The piezo-induced voltage is rectified and smoothed because the electrolysis process requires a direct voltage.

The system suffers from the effect of the deadzone since the piezo-induced voltage generated is less than E_{rev}. This means no current flow for mass deposition. The adaptive SMC controller is implemented and tasked with overcoming the deadzone non-linearity as well as generating sufficient voltage required to produce the desired mass transportation. The controller adapts to both the piezo-induced voltage and the varying reference so that the actual current tracks the reference. The performance can be seen in figures 8(a)-(c). In this sense, the piezoelectric acts as both a sensor to measure the effect of fault and an energy harvesting device.

Time varying conditions are demonstrated by applying stresses of $12MPa$, $13.2MPa$ and $14MPa$ at different time instants. The frequency is fixed at $100rad/sec$. The resulting piezo-induced voltage with changing magnitude over time is rectified and shown in figure 8(f). The sliding mode control law is tasked with adapting to changes in the piezo-induced voltage and reference. Figure 8(f) shows that the increase in load input results in increased piezo-induced voltage, and the control law (figure 8(f)) adapts by dropping its effort while ensuring proper tracking of the reference. The sudden change in the piezo-induced voltage produces spike in the tracking error which dies away as the controller adapts. Regardless of the conditions and uncertainties surrounding the implementation of a self-healing process, figure 8(d) shows that a desired response can be achieved with the control design. The control effort of both constant and time varying conditions in figures 8(c) and (f) respectively shows the effectiveness of the controller to adapt to different conditions.

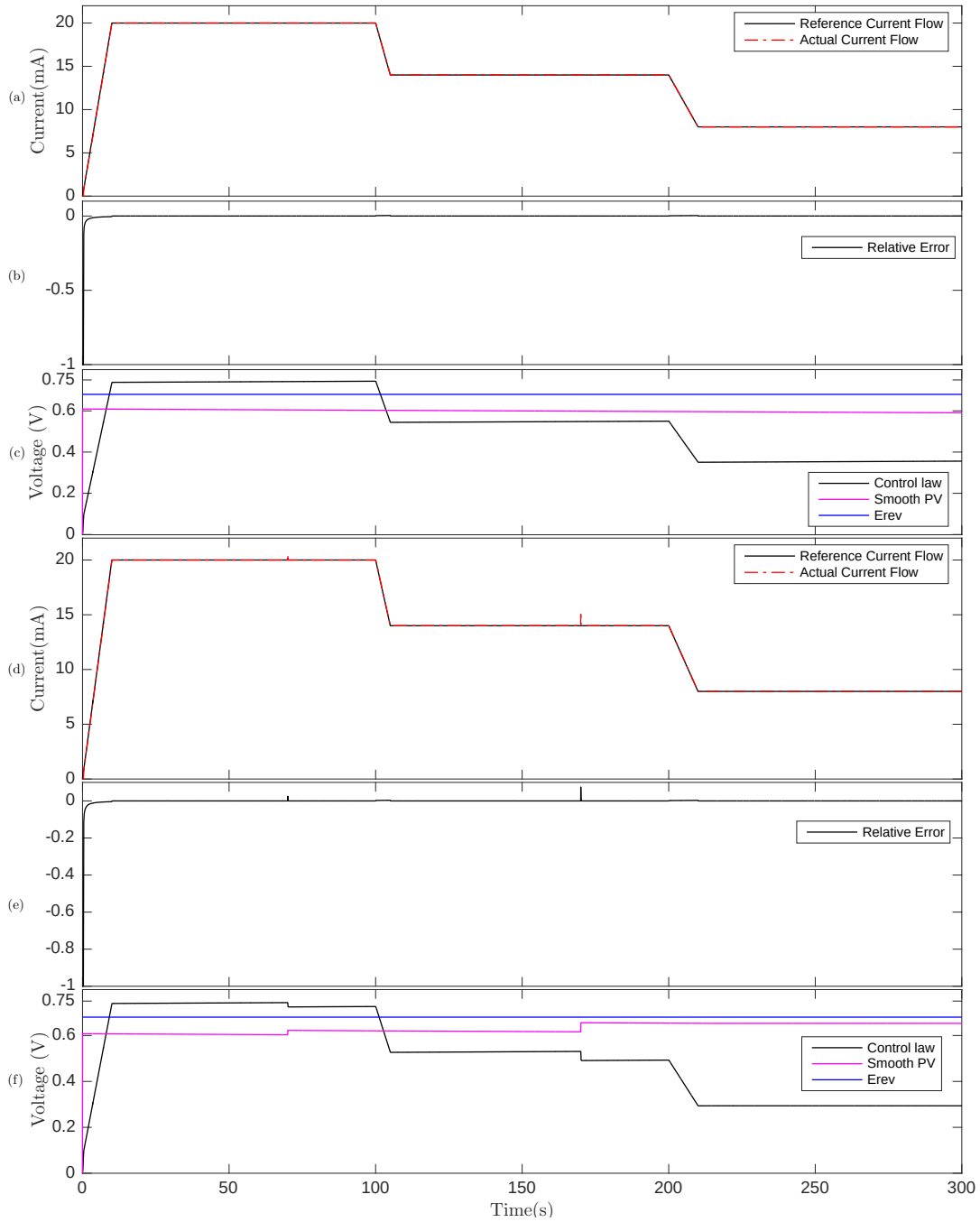

Figure 8. Adaptive SMC applied to case II which relates to a composite material system, whose self-healing mechanism is based on piezo-electrolytic drive. (a) The material is subjected to constant stress and the adaptive control law ensures that the current flow during electrolysis tracks the desired performance. (b) Relative error given as the difference between the actual and desired current divided by the desired current. (c) The control effort when subjected to constant stress. (d) The material is subjected to different stresses at different time instants and the adaptive control law adapts such that the current flow during electrolysis tracks the desired performance. (e) The relative error is given as the difference between the actual and desired current divided by the desired current. (f) As the stress changes with time, the magnitude of the piezo-induced voltage changes. Increased piezo-induced voltage will cause the adaptive control to drop its effort during tracking.

6. Conclusion

Current intrinsic and extrinsic approaches to self-healing of material systems remain predominantly passive in counteracting the effect of damage. This typically leads to a poor mismatch between the healing and the damage rate. In contrast to these self-healing approaches, this paper demonstrates the concept of active self-healing to ensure that the healing and damage rate are satisfactorily matched. This is achieved by incorporating an adaptive feedback controller to regulate the healing process. The adaptive feedback controller was designed and implemented first on a newly developed model of an electrolytic system to regulate the process. The model is based on previous experimental work [6, 38] which proposed an electromechanical material system, whose intrinsic self-healing mechanism is based on a piezo-electrolytic drive. This system suffers from an inherent non-linear deadzone which limits the performance of self-healing. The adaptive feedback controller was designed to overcome the unknown deadzone nonlinearity and to ensure a proper match between the healing and damage rate. By using sinusoidal inputs with constant and changing amplitudes, the effect of controlled self-healing system to constant and varying conditions was investigated. The control simulations successfully showed that a match between the healing rate and an estimated damage rate can be achieved. These results are an important milestone in regulating the healing rate, with reference to an estimated damage rate, of self-healing systems. The results also suggests the possibility of integrating sensing (for fault detection and prognosis), feedback control (for regulation) and energy harvesting (for electrolytic energy reduction). Importantly, an efficient way to counteract the effect of damage and improve the performance of self-healing has been shown. This work will help in making self-healing more robust and attractive for applications. Future work will focus on experimental validation of the process and integrating prognosis to predict the fault condition from sensor measurement.

References

[1] Aviation Safety Council 2005 China Airlines Flight CI-611 Crash Report Released Tech. rep. International Aviation Safety Organisation

[2] Smith M and Janet DiGiacomo C 2014 Delta Plane Loses Wing Panel During Flight URL `http://edition.cnn.com/2014/03/17/travel/delta-plane-wing-panel/`

[3] Frei R, McWilliam R and Derrick B 2013 *The International Journal of Advanced Manufacturing Technology* **69** 1033–1061

[4] Kessler M R 2007 *Proceedings of the Institution of Mechanical Engineers, Part G: Journal of Aerospace Engineering* **221** 479–495

[5] Blaiszik B, Kramer S, Olugebefola S, Moore J, Sottos N and White S 2010 *Annual Review of Materials Research* **40** 179–211

[6] Soroushian P, Nassar R U D and Balachandra A M 2012 *Journal of Intelligent Material Systems and Structures* **24** 441–453

[7] Trask R S, Norris C J and Bond I P 2013 *Journal of Intelligent Material Systems and Structures* **25** 87–97

[8] Yuan Y C, Yin T, Rong M Z and Zhang M Q 2008 *Express Polymer Letters* **2** 238–250

[9] Zemskov S V, Jonkers H M and Vermolen F J 2012 *Journal of Intelligent Material Systems and Structures* **25** 4–12
[10] Yue H B, Fernández-Blázquez J P, Beneito D F and Vilatela J J 2014 *Journal of Materials Chemistry A* **2** 3881
[11] Chen X, Wudl F, Mal A, Shen H and Nutt S 2003 *Macromolecules* **36** 1802–1807
[12] Chen X, Dam M, Ono K, Mal A and Shen H 2002 *Science* **295** 1698–1702
[13] Zhong N and Post W 2015 *Composites Part A: Applied Science and Manufacturing* **69** 226–239
[14] Hayes S, Jones F and Zhang W 2006 *In Proceedings of 15th US National Congress of Theoretical and Applied Mechanic*
[15] Hayes S, Jones F, Marshiya K and Zhang W 2007 *Composites Part A: Applied Science and Manufacturing* **38** 1116–1120
[16] Luo X, Ou R and Eberly D 2009 *Applied Materials & Interfaces* **1** 612–620
[17] Keller M W, White S R and Sottos N R 2007 *Advanced Functional Materials* **17** 2399–2404
[18] Yeom C, Kim Y and Lee J 2002 *Journal of Applied Polymer Science* **84** 1025–1034
[19] Yeom C and Oh S 2000 *Journal of Applied Polymer Science* **78** 1645–1655
[20] Brown E, Kessler M, Sottos N and White S 2003 *Journal of Microencapsulation* **20** 719–730
[21] Mergheim J and Steinmann P 2013 *Computational Mechanics* **52** 681–692
[22] Dong B, Wang Y, Fang G, Han N, Xing F and Lu Y 2015 *Cement and Concrete Composites* **56** 46–50
[23] Jones A S, Rule J D, Moore J S, Sottos N R and White S R 2007 *Journal of the Royal Society, Interface / the Royal Society* **4** 395–403
[24] Mirabedini S, Dutil I, Gauquelin L, Yan N and Farnood R 2015 *Progress in Organic Coating* **85** 168–177
[25] Song Y, Lee K, Kim D and Chung C 2016 *Sensors and Actuators B: Chemical* **222** 1159–1165
[26] Huyang G, Debertin A and Sun J 2016 *Materials & Design* **94** 295–302
[27] Wu J, Weir M D, Zhang Q, Zhou C, Melo M A S and Xu H H 2016 *Dental Materials* **32** 294–304
[28] Wertzberger B E, Steere J T, Pfeifer R M, Nensel M A, Latta M A and Gross S M 2010 *Journal of Applied Polymer Science* **118** 428–434
[29] White S R, Sottos N R, Geubelle P H, Moore J S, Kessler M R, Sriram S R, Brown E N and Viswanathan S 2001 *Nature* **409** 794–797
[30] Zhu Y, Yin T, Ren J, Liu C, Fu D and Ge L 2016 *RSC Advances* **6** 12100–12106
[31] Minakuchi S, Sun D and Takeda N 2014 *Smart Materials and Structures* **23** 115014
[32] Hurley D and Huston D 2011 *Smart Materials and Structures* **20** 025010
[33] Trask R, Bond I and Norris C 2011 Stimuli Triggered Deployment of Bio-Inspired Self-Healing Functionality *Conference on Smart Materials, Adaptive Structures and Intelligent Systems, Volume 2* (ASME) pp 753–758
[34] Toohey K, Sottos N, Lewis J, Moore J and SR White 2007 *Nature Materials* **6** 581–585
[35] Toohey K, Sottos N and White S 2009 *Experimental Mechanics* **49** 707–717
[36] Hurley D A and Huston D R 2011 Self-Sealing Pneumatic Pressure Vessel With Passive and Active Methods *Pressure Vessels and Piping Conference: Volume 6* (ASME) pp 107–112
[37] Wang Q and Wu N 2012 *Smart Materials and Structures* **21** 013001
[38] Sayayr M, Weerasiri R R, Balachandra A M and Soroushian P 2014 *Journal of Applied Polymer Science* **131** 40620
[39] McEvoy M and Correll N 2015 *Science Magazine* **347** 1378
[40] Ye X J, Song Y X, Zhu Y, Yang G C, Rong M Z and Zhang M Q 2014 *Composites Science and Technology* **104** 40–46
[41] Hall J, Qamar I P S, Rendall T C S and Trask R S 2015 *Smart Materials and Structures* **24** 037002
[42] Lee A, Wang Y and Inman D 2014 *Journal of Vibration and Acoustics* **136**
[43] Feenstra J, Granstrom J and Sodano H 2008 *Mechanical Systems and Signal Processing* **22** 721–734
[44] Satkoski C 2011 *Journal of Dynamic Systems, Measurement, and Control* **133** 051011
[45] Liu J and O'Connor W 2014 *Smart Materials and Structures* **23** 025005

[46] Corr L R and Clark W W 2002 *Smart Materials and Structures* **11** 370–376
[47] Hou S, Zhang H B and Ou J P 2012 *Smart Materials and Structures* **21** 105035
[48] Shen M, Bennett N, Ding Y and Scott K 2011 *International Journal of Hydrogen Energy* **36** 14335–14341
[49] Isermann R, Lachmann K H and Matko D 1992 *Adaptive Control Systems* (Prentice-Hall International (UK) Ltd)
[50] Harris C J and Billings S 1985 *Self-Tuning and Adaptive Conrol: Theory and Applications* 2nd ed (Peter Peregrinus Ltd., London UK)
[51] Krstic M, Kokotovic P V and Kanellakopoulos I 1995 *Nonlinear and Adaptive Control Design* 1st ed (John Wiley & Sons, Inc. New York)
[52] Slotine J and Li W 1991 *Applied Nonlinear Control* (Prentice-Hall International, Inc)
[53] Su C and Stepanenko Y 2000 *IEEE Transactions on Automatic Control* **45** 2427 – 2432
[54] Wang X S, Su C Y and Hong H 2004 *Automatica* **40** 407–413
[55] Jasim I 2013 *Proceedings of the Institution of Mechanical Engineers, Part I: Journal of Systems and Control Engineering* **227** 184–197
[56] Nunes-Pereira J, Ribeiro S, Ribeiro C, Gombek C, Gama F, Gomes A, Patterson D and Lanceros-Méndez S 2015 *Polymer Testing* **44** 234–241
[57] Recker D, Kokotovic P, Rhode D and Winkelman J 1991 *Proceedings of the 30th IEEE Conference on Decision and Control* 2111 – 2115